Tropospheric warming over the North Indian Ocean caused by the South Asian anthropogenic aerosols: possible impact on the upper troposphere and lower stratosphere

Suvarna Fadnavis[1*], Prashant Chavan[1], Akash Joshi[2], Sunil Sonbawne[1], Asutosh Acharya[3], Panuganti C S. Devara[4], Alexandru Rap[5], Felix Ploeger[6] and Rolf Müller[6]

[1]Indian Institute of Tropical meteorology, MoES, Pune, India

[2]Indian Institute of Technology, Kharagpur, India

[3]Indian Institute of Technology, Bhubneshwar, India

[4]Centre of Excellence in ACOAST/ACESH, Amity University Haryana (AUH), Gurugram 122413, India

[5]School of Earth and Environment, University of Leeds, Leeds, United Kingdom

[6]Forschungszentrum Jülich GmbH, IEK-7, Jülich, Germany

Corresponding author: Suvarna Fadnavis

Corresponding author email: suvarna@tropmet.res.in

Abstract

Atmospheric concentrations of South Asian anthropogenic aerosols and their transport play a key role in the regional hydrological cycle. Here, we use the ECHAM6-HAMMOZ chemistry-climate model to show the structure and implications of the transport pathways of these aerosols during spring (March-May). Our simulations indicate that large amounts of anthropogenic aerosols are transported from South Asia to the North Indian Ocean and Western Pacific. These aerosols are then lifted into the upper troposphere and lower stratosphere (UTLS) by the ascending branch of the Hadley circulation, where they enter the westerly jet. They are further transported to the Southern Hemisphere (~15° S – 30° S), and downward (320 – 340K) via westerly ducts over the tropical Atlantic (5° S – 5° N, 10° W – 40° W) and Pacific (5° S – 5° N, 95° E – 140° E). The carbonaceous aerosols are also transported to the Arctic leading to local heating (0.08 – 0.3 K month^{-1}, an increase by 10 – 60 %).

The presence of anthropogenic aerosols causes a negative radiative forcing (RF) at the TOA (-0.90±0.089 W m^{-2}) and surface (-5.87±0.31 W m^{-2}) and atmospheric warming (+4.96±0.24 W m^{-2}) over South Asia (60° E - 90° E, 8° N - 23° N), except over the Indo-Gangetic plain (75° E - 83° E, 23° N - 30° N) where RF at the TOA is positive (+1.27±0.16 W m^{-2}) due to large concentrations of absorbing aerosols. The carbonaceous aerosols lead to in-atmospheric heating along the aerosol column extending from the boundary layer to the upper troposphere (0.1 to 0.4 K $month^{-1}$, increase by 4 – 60 %) and in the lower stratosphere 40° S – 90° N (0.02 to 0.3 K $month^{-1}$, increase by 10 – 60 %). The increase in tropospheric heating due to aerosols results in an increase in water vapor concentrations, which are then transported from the North Indian Ocean-Western Pacific to the UTLS over 45º S – 45º N (increasing water vapor by 1 - 10 %).

Keywords: South Asian Anthropogenic aerosols; warming over the Arabian Sea; transport of aerosols and water vapor to the UTLS in spring.

1. Introduction

Understanding the variability of anthropogenic aerosol loading over the North Indian Ocean is of utmost importance since (1) it regulates the Asian hydrological cycle via modulating atmospheric convection, heating rates, and moisture transport (Ramanathan et al., 2005; Corrigan et al., 2008; Budhavant et al., 2018, Meehl et al., 2008), and (2) it leads to adverse impacts on marine ecosystems (Mahowald et al., 2018; Collins et al., 2019). Several observations indicate that the aerosol loading over the North Indian Ocean during the spring season is strongly influenced by South Asian aerosols. Aircraft measurements during the Indian Ocean Experiment (INDOEX) (February–March 1999) showed the presence of a thick layer (surface to 3.2 km) of anthropogenic aerosols (BC~14 %, sulfate 34 %, ammonium 11 %) over the North Indian Ocean (Dickerson et al., 2002; Mayol-Bracero et al., 2002) with sources over South Asia. Several other in situ observations, e.g. over the Maldives during November 2014 – March 2015, show that air masses arising from the Indo-Gangetic Plain contain very high amounts (97 %) of the elemental carbon in the PM_{10} in the fine mode. (Bhudhvant et al., 2018). Observations from the Geosphere-Biosphere Programme over the Bay of Bengal during spring (March 2016) also show abundant anthropogenic aerosols (sulfate and nitrate) having sources over the Indo-Gangetic plain (Nair et al., 2017).

The aerosol loading over South Asia has been increasing at an alarming rate (rate of increase in AOD 0.004 per year during 1988 – 2013) (Babu et al., 2013). For the last two decades, the AOD increase (by 12 %) over South Asia has been attributed to the strong increase in anthropogenic aerosols (sulfate, black carbon, and organic carbon), while natural aerosol remained unchanged (Ramachandran et al., 2020a). The major sources of anthropogenic aerosols are the combustion of domestic fuels, industrial emissions, transportation, and open burning (Paliwal et al., 2016). The growth of the economy of India led to a 41 % increase in

BC and 35 % in OC from 2000 to 2010 (Lu et al., 2011). The emissions of sulfur dioxide (SO_2) which leads to the production of sulfate aerosols have doubled during 2006 – 2017 (Fadnavis et al., 2019). Figure 1 a-c shows the annual mean emission of BC, OC, and sulfate aerosols over South Asia in 2016 from AEROCOM-ACCMIP-II emission inventory (discussed in section 2.1). It shows high emissions over the Indo-Gangetic Plain (BC 7×10^{-12}– 17×10^{-12} Kg m^{-2} S^{-1}, OC: 25×10^{-12} - 70×10^{-12} Kg m^{-2} S^{-1}, sulfate: 2×10^{-12} - 5×10^{-12}Kg m^{-2} S^{-1}). Higher amounts of aerosols over the Indo-Gangetic Plain are associated with densely populated regions and industrial and vehicular emissions (Karambelas et al., 2018, Fadnavis et al., 2019). Past studies also show substantially higher amounts of aerosols over North India compared to the rest of the Indian region (Ramachandran et al., 2020b, Fadnavis et al., 2013, 2017a, 2017b). Over the Indo-Gangetic plain, these emissions show a peak in spring (Fig. 1d), with increases for BC of 0 – 3 %, OC 0 – 8.7 %, and sulfate 0 – 0.2 %, compared to annual means. This peak in emissions in spring is to a large extent driven by springtime agricultural crop burning and biomass burning activity (Chavan et al., 2021).

While the presence of sulfate aerosols leads to a cooling of the atmosphere below due to their strong scattering properties, carbonaceous aerosols produce atmospheric warming via absorption of solar radiation (Fadnavis et al., 2019, Penner et al., 1998). Previous studies showed that the doubling of carbonaceous aerosols loading over South Asia (10° S – 50° N, 65° E – 155° E) led to significant atmospheric warming (in-atmospheric RF 5.11W m^{-2}, Fadnavis et al. 2017b).

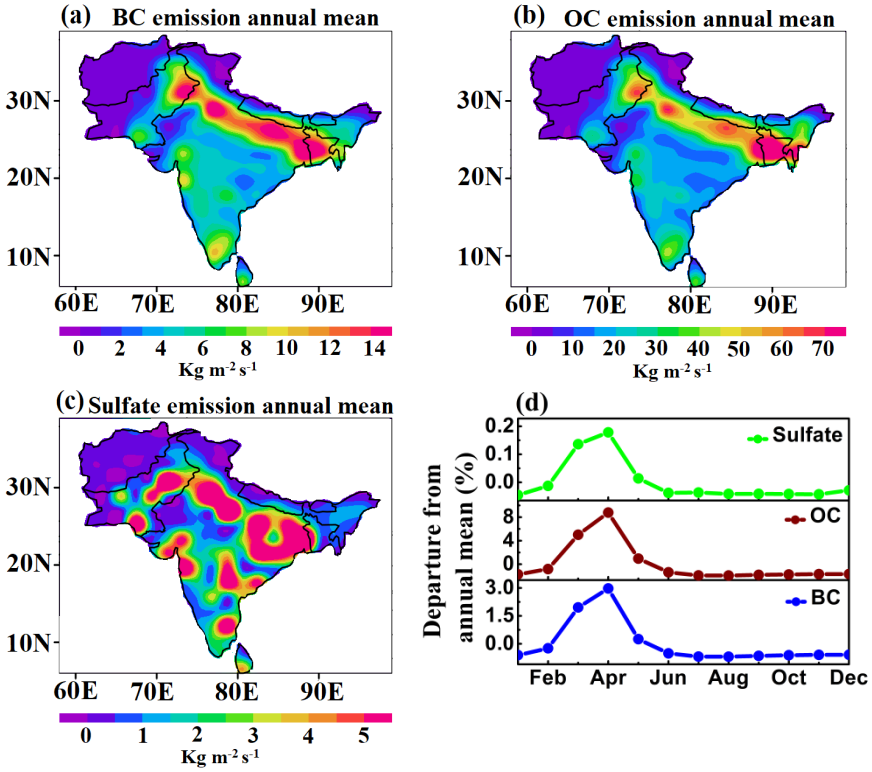

Figure 1: Spatial distribution for the year 2016 annual mean total emission (kg m^{-2} S^{-1}) of (a) BC, (b) OC, (c) Sulfate aerosols from AEROCOM-ACCMIP-II emission inventory, (d) time series of monthly departure from annual mean total emissions (%) of BC, OC, and Sulfate aerosols averaged over Indo-Gangetic plain (23° N – 30° N, 78° E – 90° E).

During spring, the prevailing convective instability over the Bay of Bengal and the Arabian Sea transports aerosol from the boundary layer to the upper troposphere (Romatschke and Houze, 2011). Airborne observations during winter and spring, e.g. the Civil Aircraft for Regular Investigation of the Atmosphere based on an Instrument Container (CARIBIC) in March 1999 and January 2001 (Papaspiropoulos et al., 2002), and the Indian Ocean Experiment (INDOEX) in February-March 1999 show elevated aerosol amounts near 8 – 12 km over the Indian Ocean and South Asia (De Reus et al., 2001). Recently, using a set of model simulations, Chavan et al., (2021) reported the transport of biomass burning aerosols to the upper troposphere by convection in spring 2013.

111 Here, we investigate the source of the very large aerosol loading over the Arabian Sea
112 during spring and, their vertical transport to the UTLS. We show these aerosols produce
113 atmospheric warming leading to enhanced water vapor that is transported to the UTLS. Once
114 in the lower stratosphere, aerosols and water vapour are transported to the Southern hemisphere
115 (~45º S), with implications on tropospheric temperatures and stratospheric ozone
116 concentrations. For this purpose, we performed a series of five simulations using the
117 ECHAM6-HAMMOZ model in order to investigate the impact of changes in anthropogenic
118 aerosol over South Asia. The paper is structured as follows: the ECHAM6-HAMMOZ model
119 simulations are provided in section 2, in section 3 we discuss the results on the transport of
120 South Asian aerosols to the North Indian Ocean, radiative forcing, transport into the UTLS,
121 and associated impacts on heating rates, while conclusions are summarised in section 4.

122 **2. Model simulations**

123 **2.1 ECHAM6-HAMMOZ experimental set-up**

124 We use the state of the art aerosol–chemistry-climate model ECHAM6–HAMMOZ. It
125 comprises of the general circulation module ECHAM6, coupled to the aerosol and cloud
126 microphysics module Hamburg (HAM) (Stier et al., 2005; Tegen et al., 2019). HAM predicts
127 the nucleation, growth, evolution, and sinks of sulfate, black carbon (BC), organic carbon
128 (OC), sea salt (SS), and mineral dust (DU) aerosols. The size distribution of the aerosol
129 population is described by seven log-normal modes (Nucleation mode, soluble and insoluble
130 Aitken, soluble and insoluble accumulation and soluble and insoluble coarse modes) (Stier
131 et al., 2005; Zhang et al., 2012; Tegen et al., 2019). Moreover, HAM explicitly simulates the
132 impact of aerosol species on cloud droplet and ice crystal formation according to prescribed
133 microphysical properties. Aerosol particles can act as cloud condensation nuclei or as kernel
134 for ice-nucleating particles. Other relevant cloud microphysical processes such as

evaporation of cloud droplets, sublimation of ice crystals, ice crystal sedimentation, and detrainment of ice crystals from convective cloud tops are simulated interactively (Neubauer et al., 2014). The anthropogenic and fire emissions of sulfate, black carbon (BC), and organic carbon (OC) are based on the AEROCOM-ACCMIP-II emission inventory. Other details of the model and emissions are reported by Fadnavis et al. (2017a, 2019, 2021a, b).

The model simulations are performed at a T63 spectral resolution corresponding to 1.875°x1.875° in the horizontal dimension, while the vertical resolution is described by 47 hybrid σ−p levels from the surface up to 0.01 hPa (approx. 80 km). The simulations have been carried out with a time step of 20 min. Monthly varying Atmospheric Model Inter-comparison Project (AMIP) sea surface temperature (SST) and sea ice cover (SIC) (Taylor et al., 2000) were used as lower boundary conditions.

We performed five model experiments: (1) a control (CTL) simulation where all aerosol emissions are included and four perturbed experiments where (2) all anthropogenic aerosol emissions (black carbon, organic carbon, and sulfate) are switched off over South Asia (75° E – 100° E, 8° N – 40° N, see Fig. 1) during the study period (2001 – 2016) (referred to as Aerooff), (3) only anthropogenic black carbon emissions (BC) switched off during the study period, (BCoff), (4) only anthropogenic organic carbon (OC) emissions switched off (OCoff) during the study period, and (5) only anthropogenic sulfate aerosol emissions switched off (Suloff) during the study period (see Table 1). All simulations were performed from 1 January 2001 to December 2016 from stabilized initial fields created after a model integration for one year. Dust emission parameterization is the same in all the simulations and is based on Tegen et al. (2002). The analysis is performed for spring (March – May) averaged for the period 2001 – 2016. We compare the CTL with Aerooff, BCoff, OCoff, and Suloff simulations to understand (1) transport path ways of South Asian anthropogenic aerosols, and (2) their impact over the Indian region, and UTLS (340K – 400K). We compare AOD from CTL simulations

with MISR and MODIS data (section S1). The model performance against MISR and MODIS (Kahn et al., 2007) for the spring season is discussed in section S2 from Fig. S1. We use the 2 PV contour in mid-latitudes and the 380 K isentrope in the tropics as an estimate of the location of the dynamical tropopause (Holton et al., 1995). Note that the PV value at the dynamical tropopause is often somewhat higher than 2 PV and exhibits a certain variability (Kunz et al., 2011).

Table -1: Details of ECHAM6-HAMMOZ model simulations performed in this study.

Experiment name	Duration	Aerosol species on/off	Boundary conditions
CTL	2001 – 2016	All aerosols species globally, as per AEROCOM-ACCMIP-II emission inventory.	AMIP Sea surface temperature and sea ice concentration.
Aerooff	2001 – 2016	Anthropogenic BC, OC, and sulfate aerosols switch off over South Asia during 2001 – 2016.	AMIP Sea surface temperature and sea ice concentration.
BCoff	2001 – 2016	Anthropogenic BC aerosols switch off over South Asia during 2001 – 2016.	AMIP Sea surface temperature and sea ice concentration.
OCoff	2001 – 2016	Anthropogenic OC aerosols switch off over South Asia during 2001 – 2016.	AMIP Sea surface temperature and sea ice concentration.
Suloff	2001 – 2016	Anthropogenic sulfate aerosols switch off over South Asia during 2001 – 2016.	AMIP Sea surface temperature and sea ice concentration.

3. Results and discussions

3.1 Transport of South Asian aerosols to the North Indian Ocean

The spatial distribution of AOD anomalies from the CTL-Aerooff simulation shows positive anomalies of AOD extending from South Asia to the Arabian Sea and the North Bay of Bengal (10º N - 20º N) (Fig. 2a). The wind vectors indicate that these are transported from the Indo-

Gangetic plain to the Arabian Sea, the Bay of Bengal and Western Pacific. The transported aerosols enhanced the AOD by 0.18 - 0.8 (30 - 80 %) over the North Bay of Bengal and by 0.02 - 0.12 (20 - 60 %) over the Arabian Sea. This is consistent with previous studies where 50 - 60 % enhancements in the AOD over the tropical Indian Ocean due to anthropogenic aerosols have been reported (Satheesh et al. 2000; Jose et al. 2020). Chemical analysis of aerosols observed over the south-eastern coastal Arabian Sea also shows the dominance of anthropogenic aerosols having sources over the Indian region (73 %) (Aswini et al., 2020). Analysis of MODIS satellite observations (2003 – 2017) likewise shows that anthropogenic sources contributed ~60 – 70% to the aerosol loading over the east coast and west coast of India (Jose et al. 2020).

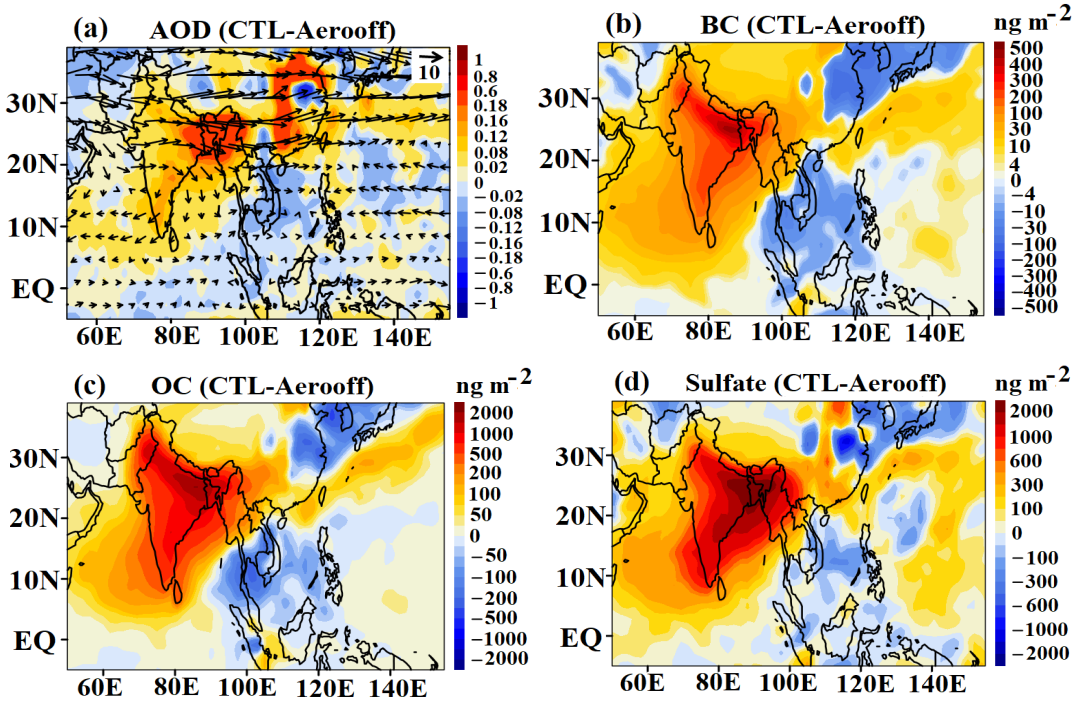

Figure 2: Spatial distribution of (a) AOD anomalies averaged for spring during 2001 – 2016 (CTL - Aerooff), and anomalies of tropospheric column of (b) BC, (c) OC, and (d) sulfate aerosols (ng m^{-2}) (CTL-Aerooff). The vectors in Fig.2a indicate winds (m s^{-1}) at 850 hPa.

The distribution of anomalies of the tropospheric column of BC, OC, and sulfate aerosols also indicates that these aerosols are transported from South Asia to the Bay of Bengal and the Arabian Sea (Fig. 2b-d). Enhancement of sulfate and OC aerosol (50 – 2000 ng m^{-2}) is higher

than BC (4 – 500 ng m^{-2}) over the South Asian region (Fig. 2b-d). The total carbonaceous aerosol (BC and OC together) dominates over the sulfate aerosols. These anthropogenic aerosols over the tropical Indian Ocean affect the radiation budget and cloud cover over the Indian Ocean (Satheesh et al., 2000; McFarquhar and Wang, 2006).

3.2. Radiative forcing

The anthropogenic aerosols over the tropical Indian Ocean affect the radiation budget and cloud cover (McFarquhar and Wang, 2006). Here, we discuss the impact of South Asian anthropogenic aerosols on RF. Figures 3a-c show anomalies in net RF at the TOA, surface, and in-atmosphere (TOA - surface) for Aerooff simulations (CTL - Aerooff). The anthropogenic aerosols have produced a cooling at the TOA (except over the Indo-Gangetic plain) and at the surface (see Fig. 3a-b). The simulated RF values over the Arabian Sea (55° E – 70° E, 8° N – 20° N), Bay of Bengal (88° E – 92° E, 12° N – 20° N), and Indo-Gangetic Plain (75° E – 83° E, 26° N – 30° N) are tabulated in Table-S1. The RF estimates show that the aerosols have produced cooling at the TOA and surface over the Arabian Sea (TOA: -0.72±0.14 W m^{-2}, surface:-3.0±0.28 W m^{-2}), Bay of Bengal (TOA:-1.24±0.15 W m^{-2}, surface: -5.14±0.44 W m^{-2}), and in-atmospheric warming over the above regions (Arabian Sea +2.27±0.19 W m^{-2}; Bay of Bengal: +3.89±0.30 W m^{-2}) (Fig. 3 c). The Indo Gangetic Plain shows positive anomalies of RF at the TOA (+1.27±0.16 W m^{-2}), negative at the surface (-11.16±0.50 W m^{-2}), and an atmospheric warming of +12.44±0.42 W m^{-2}. In agreement with our results, previous studies have reported negative RF at the surface and TOA, and atmospheric warming over the North Indian Ocean caused by enhanced anthropogenic aerosol. For example, Pathak et al. (2020) reported negative aerosol RF at the TOA (-2 to -4 W m^{-2}) over the Bay of Bengal and the Arabian Sea during spring 2009 - 2013. The clear sky aerosol direct radiative forcing estimated from measurements during the INDOEX experiment (January to March in 1999) over the North Indian Ocean also show similar results (TOA: -7 W m^{-2}, surface: -23 W m^{-2}, and in-

atmosphere: +16 W m^{-2}) (Ramanathan et al., 2001). There is a large variation in the magnitude of RF (at the TOA, surface, and in-atmosphere) reported from observations and our model simulations. This may be due to different regions and different time periods and the relatively coarse model resolution. The observation-based studies attribute positive in-atmospheric radiative forcing to absorbing aerosols (especially black carbon) that lead to a heating of the atmosphere (Rajeev and Ramanathan, 2001; Satheesh et al., 2002).

The analysis of the perturbed model experiments indicates that anthropogenic BC aerosols (Fig. 3d-f) have produced a warming at the TOA (Arabian Sea: 1.24±0.13 W m^{-2}, Bay of Bengal: 1.54±0.26 W m^{-2}, Indo-Gangetic Plain: 4.33±0.17 W m^{-2}) and cooling at the surface (Arabian Sea: -2.56±0.25 W m^{-2}, Bay of Bengal: -3.70±0.49 W m^{-2}, Indo-Gangetic Plain:-9.27±0.37 W m^{-2}). OC (Fig. 3g-i) and sulfate (Fig. 3j-l) aerosols have produced significant cooling at the TOA (OC: -0.21±0.13 to -0.44±0.15 W m^{-2}; Sulfate: -1.55±0.16 to -2.14±0.17 W m^{-2}) and surface (OC: -0.49±0.31 to -2.56±0.45 W m^{-2}, Sulfate: -1.19±0.24 to -2.67±0.36 W m^{-2}) over the above regions (listed in Table-S1). Figures 3d, 3g, and Fig. 3j further confirm our finding that the positive anomalies of radiative forcing in the Indo-Gangetic plain are due to BC aerosols because of its absorbing property. All the aerosols produce in-atmospheric warming over the Indian region (Fig. 3c, 3f, 3i, 3l) and the North Indian Ocean (Fig. 3c, 3f, 3i). The atmospheric warming over the Arabian Sea and Bay of Bengal is due to BC and OC aerosols with larger contributions by the BC aerosols.

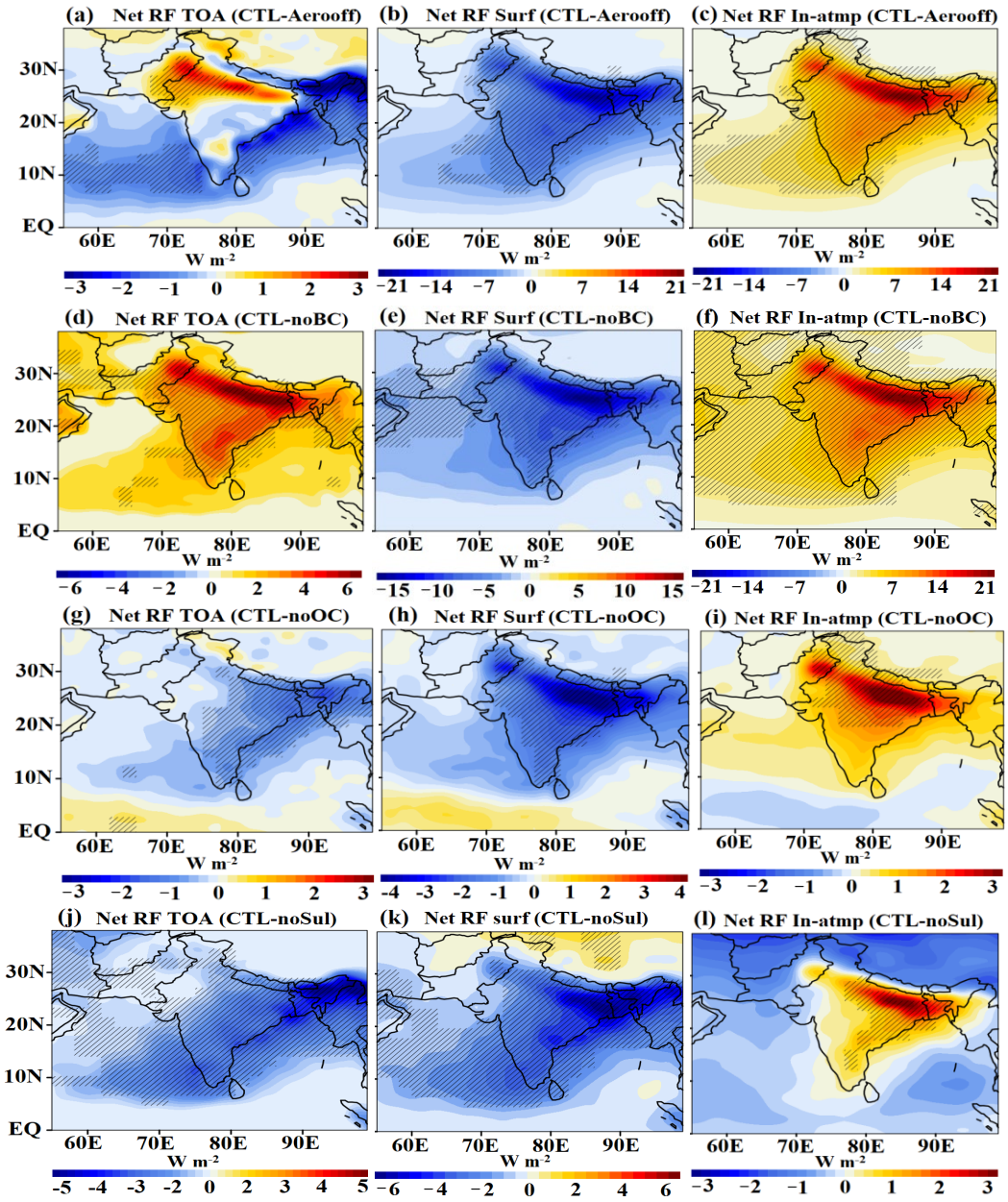

Figure 3: Spatial distribution of net aerosol radiative forcing (CTL - Aerooff) (W m^{-2}) averaged for spring for the years 2001 – 2016 (a) TOA, (b) same as (a) but for surface, (c) same as (a) but for in-atmosphere (TOA - surface), (d) spatial distribution of radiative forcing at the TOA (CTL – BCoff) averaged for spring for the years 2001 – 2016, (e) same as (d) but for surface, (f) same as (d) but for in-atmosphere (TOA - surface), (g) spatial distribution of radiative forcing at the TOA (CTL - OCoff) averaged for spring during 2001 – 2016, (h) same as (g) but for surface, (i) same as (h) but for in-atmosphere (TOA - surface), (j) spatial distribution of radiative forcing at the TOA (CTL - Suloff) averaged for spring during 2001 – 2016, (k) same as (j) but for surface, (l) same as (k) but for in-atmosphere (TOA - surface). The hatched lines in figure a-l indicate 99% confidence level for the mean differences.

3.3. Transport of Asian anthropogenic aerosols into the UTLS

Further, we investigate the vertical distribution of aerosols that are transported to the North Indian Ocean. This analysis is performed on the isentropic levels, since past studies show that air mass transport from the troposphere to the stratosphere occurs largely along quasi-isentropic surfaces (Ploeger et al., 2017; Yan et al., 2021). In spring, Asian aerosols are transported partly to the Arabian Sea and Bay of Bengal region and partly to the Western Pacific (Fig. 2a-d). Hence the meridional section is shown over the Indian Ocean and western Pacific region (30° E – 140° E) (Fig. 4 a-c). The vertical distribution of BC, OC, and sulfate aerosols indicates that these aerosols are transported from the boundary layer (10º N – 30º N) into the UTLS (340 – 400K) (Fig. 4a-c and Fig. S2). In the UTLS, at ~350K – 390K they are transported southward (~ 30º S) and downward (~320 K – 340 K). The quasi-isentropic transport occurs via two pathways (1) over Africa (20º E – 60º E) and (2) over the East Indian Ocean and Western-Pacific (95º E – 140º E) (Fig. 4d-f). The downward penetration of aerosols (BC, OC, and sulfate) in the Southern Hemisphere (15º S – 30º S) to 320K – 340K via the above mentioned two pathways is also evident in Figure 4 g-i.

In the following, we further explore processes responsible for inter-hemispheric transport. Our analysis indicates that the Hadley circulation (Fig. 5a and Fig. S3) with its ascending branch over the Indian Ocean and adjoining region (60º E – 140º E, 0 – 30º N), lifts the South Asian aerosols to the UTLS. These aerosols enter the westerly jet (Fig. 4 d-f).

The distribution of zonal winds in Fig. 5b shows transport into the southern hemisphere preferentially in regions of equatorial westerly winds, so-called "westerly duct" regions (Waugh and Polvani, 2000; Yan et al., 2021), where Rossby-wave breaking occurs (Fig. 5b and Fig. S4). This is consistent with findings from Frederiksen et al. (2018) who have also shown interhemispheric transport of CO_2 via Pacific and Atlantic westerly ducts during the

spring season. Fig. 5c shows that changes in South Asian aerosols concentrations cause a shift in the Pacific duct. Thus interhemispheric transport occurs through (1) an Atlantic duct and (2) a slightly shifted Pacific duct (5 ° S – 5 ° N, 50 ° E – 140 ° E), i.e. over the Indian-Ocean-Western Pacific region (also see Fig. 4 d-f). The shift in Pacific duct in a response to South Asian aerosol changes is likely due to higher Rossby wave bearing near south Asia. The geopotential (Fig 5d) and potential vorticity (Fig. S5) anomalies (CTL-Aerooff) show Rossby wave breaking near the Indian-Ocean-Western Pacific region that could lead to Southern hemispheric transport through the Indian-Ocean-Western Pacific region path (Fig 5 c-d). In addition, the interhemispheric transport is also likely influenced by the monthly migration and the strength of the Hadley circulation (Fig. S3).

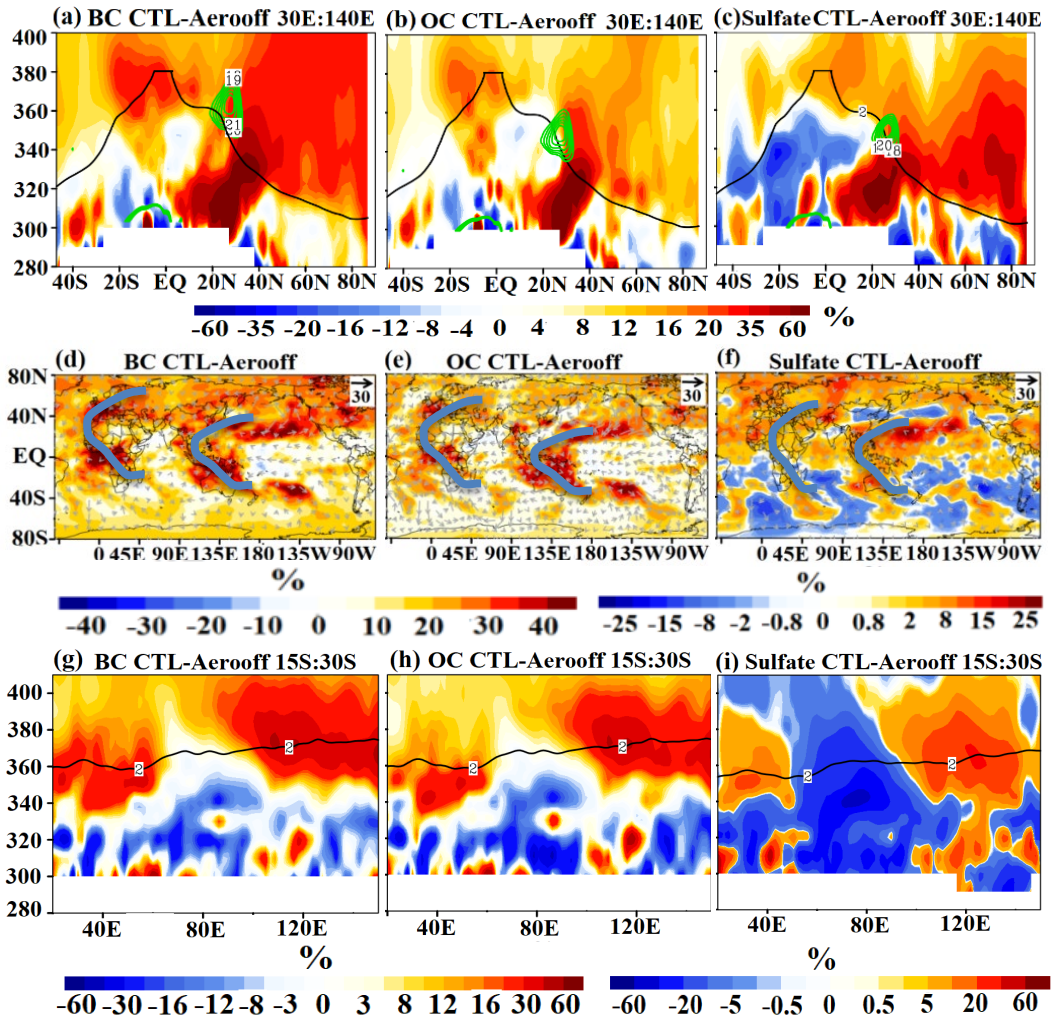

Figure 4: Meridional cross-section over Indian Ocean-western Pacific (averaged 30º E – 140º E and for the spring season for the years 2001 – 2016) of anomalies (%) (CTL-Aerooff) of (a-c) BC, OC, and sulfate aerosols. Green contours in (a-c) indicate westerly jet. Fig (d-f) spatial distribution of BC, OC and Sulfate aerosols averaged at 360 – 390K isentropic levels and the spring season for the years 2001 – 2016, vectors in Figs. a-f indicate anomalies of winds (m s^{-1}). (g-h) Zonal cross-section (averaged over 15º S – 30º S and for the spring season for the years 2001 – 2016) and for the spring season for BC, OC, and sulfate aerosols. The black line of 2 PV in (a-c and g-i) indicates the dynamical tropopause.

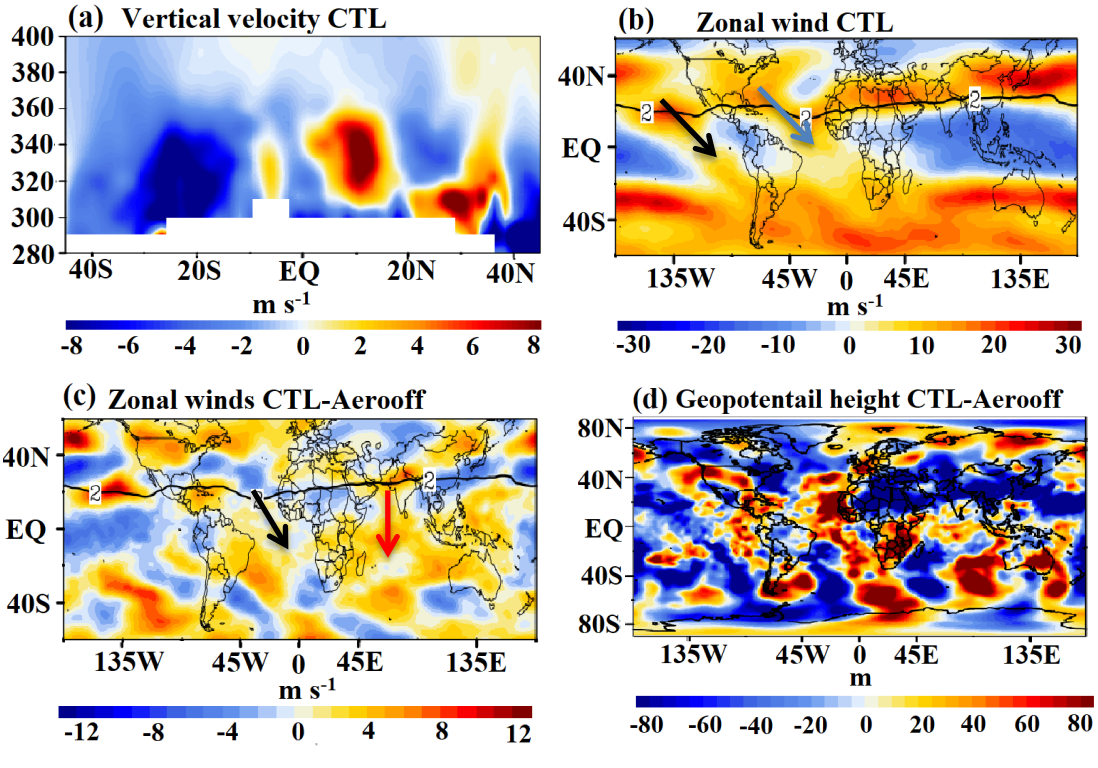

Figure 5: Meridional cross section of vertical velocities (m s^{-1}) (averaged for 65 º E – 140º E and for spring season during 2001 – 2016). Vertical velocities are scaled by 300, (b) zonal winds at 360 K isentropic level from CTL simulations, a black arrow indicates Pacific duct and blue arrow indicates Atlantic duct, (c) anomalies (CTL-Aerooff) zonal winds at 360 K isentropic level. A black arrow indicates the Atlantic duct and red arrow indicates duct over the Indian Ocean, (d) anomalies (CTL-Aerooff) of geopotential height (m) at the 340K potential temperature level. The potential vorticity (2 PVU) is indicated by the black contour in Figs. a-c.

Further, in the UTLS, South Asian aerosols are transported to the Arctic (Fig. 4 a-c). There is an aerosol enhancement in the Arctic (BC: 10 to 30 %, OC: 10 to 20 %, Sulfate: 5 to 30 %).

Our analysis shows that transport to the Arctic occurs every year in the UTLS which causes heating in the lower stratosphere (380 K – 400K) (see Section 3.4).

3.4. Impacts on the net heating rate and water vapour

Carbonaceous aerosols absorb solar radiation, leading to atmospheric heating, while predominately scattering aerosols such as sulfate reflect and scatter back solar radiation, therefore cooling the atmosphere below (Fadnavis et al., 2019). Here, we analyse net heating rates (short wave + long wave) induced by all the anthropogenic Asian aerosols (CTL - Aerooff). Changes in the net heating rates are induced by the aerosol changes; any changes in dynamical heating will be intrinsic. The vertical distribution of net heating rate anomalies over the North Indian Ocean and Western Pacific region (30° E – 140° E) indicates increase in heating rates in the region of elevated anthropogenic aerosols in the troposphere (0.15 to 0.4 K $month^{-1,}$ 5 – 60 %) and UTLS (0.02 to 0.3 K $month^{-1}$, 10 – 60 %) (Fig. 6a-d, Fig. 4, and Fig. S2). Heating rate anomalies estimated over the North Indian Ocean and western Pacific region from BC (CTL - BCoff), OC (CTL - OCoff), and Sulfate (CTL - Suloff) show that BC and OC aerosols produce heating in the troposphere (280K – 340K) (10° N – 40° N) (BC: 0.6 to 2 K $month^{-1}$, 10 – 50% , OC: 0.2 to 0.4 K $month^{-1}$, 0.5 – 4 %) and UTLS over Northern hemisphere (BC: 0.08 to 0.2 K $month^{-1}$, 30 – 45%, OC: 0.02 to 0.06 K $month^{-1}$, 0.2 – 1.5 %), while sulfate aerosols produce atmospheric cooling in the troposphere and UTLS -0.02 to -0.4 K $month^{-1}$ (5 – 40 %) (280 - 400K) (Fig. 6a-d). Black carbon aerosol produces higher heating than organic carbon aerosols. The shortwave heating due to BC aerosols is the major contributor to the total heating. In general, these aerosols increase heating in the troposphere extending to the lower stratosphere (400K) over the South Asian region (Fig. 6a). There is enhancement in heating rates along the path of aerosols transported to the Arctic.

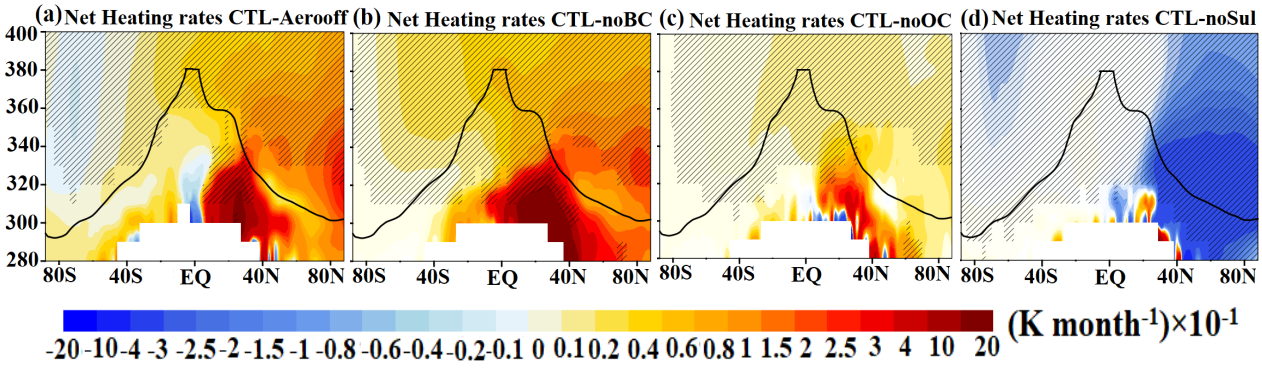

Figure 6: Meridional cross-section of heating rates (K month^{-1}) over the Indian Ocean-western Pacific (averaged 30º E – 140º E and for the spring season for the years 2001 – 2016) (a) from CTL - Aerooff simulation, (b) same (a) but from CTL - BCoff simulation (c) same (a) but from CTL -OCoff simulation, (d) same (a) but from CTL - Suloff simulation. Hatches in Figs. a-d indicate 95% significance level. A black line in Figs. a-d indicates the dynamical tropopause.

The vertical distribution of water vapor over the Indian Ocean-Western Pacific region (30º E – 140º E) (CTL - Aerooff) shows that water vapour concentrations are enhanced by 1-10% along the path of elevated aerosols (Fig. 7a and Fig. 4). In the UTLS, water vapour is transported to the southern hemisphere ~45º S. This may be due to heating caused by the Asian aerosols. The impact of BC (CTL - BCoff), OC (CTL - OCoff), and Sulfate (CTL - Suloff) on the water vapor distribution (Fig. 7 b-d) shows that BC aerosols play a major role in water vapor enhancement in the UTLS (Fig. 7 b). Water vapor enhancement by BC aerosols over the Indian Ocean-Western Pacific region is ~ 1 – 15 % (Fig. 7b). The water vapor enhancement by OC aerosols in the UTLS region is 0.8 – 15% (Fig. 7c) and by sulfate aerosols ~0.2 – 1% in pockets (Fig. 7d).

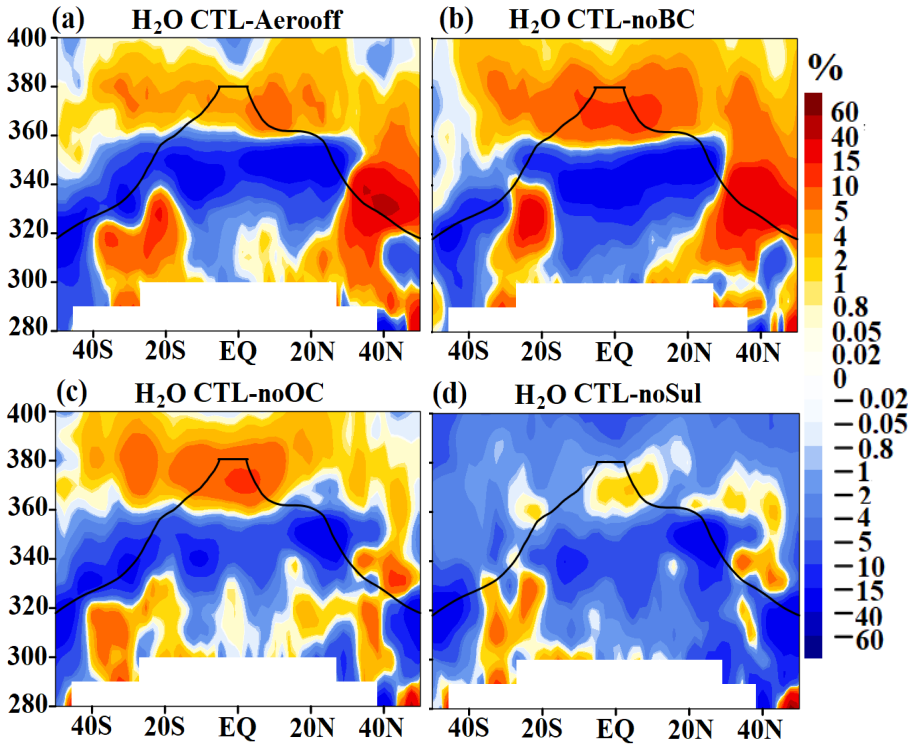

Figure 7: (a) Meridional cross-section over the Indian Ocean-western Pacific (averaged over 30° E – 140° E) of anomalies of water vapour (%) (CTL - Aerooff) the for spring season for the years 2001 – 2016, (b) same as (a) but from CTL - BCoff simulations, (c) same as (a) but from CTL - OCoff simulations, (d) same as (a) but from CTL - Suloff simulations. A black line in Figs. a-d indicates the dynamical tropopause.

Although the focus of the manuscript is on the transport of aerosols during the spring season, it should be noted that the anthropogenic South Asian aerosols are also transported to the UTLS during the monsoon season (Shindell et al., 2008, Fadnavis et al., 2013, 2017, 2019, Zheng et al., 2021). Annual distribution anomalies of aerosols (average of BC, OC, and sulfate) show the transport of aerosols into the UTLS during the spring and monsoon seasons (April to September) from South Asian region (Fig. 8a). In the lower stratosphere, these aerosols persist for a few months (Fig. 8a) thus their effect will be seen for an extended time. These aerosols enhance tropospheric heating thereby transporting elevated water vapour into the lower stratosphere (Fig. 8b). Figure 8a also shows the transport of aerosols into the lower stratosphere

during spring and the monsoon seasons (March-September). The aerosol induced enhanced water vapour also shows enhancement in the lower stratosphere during the same time (Fig. 8b).

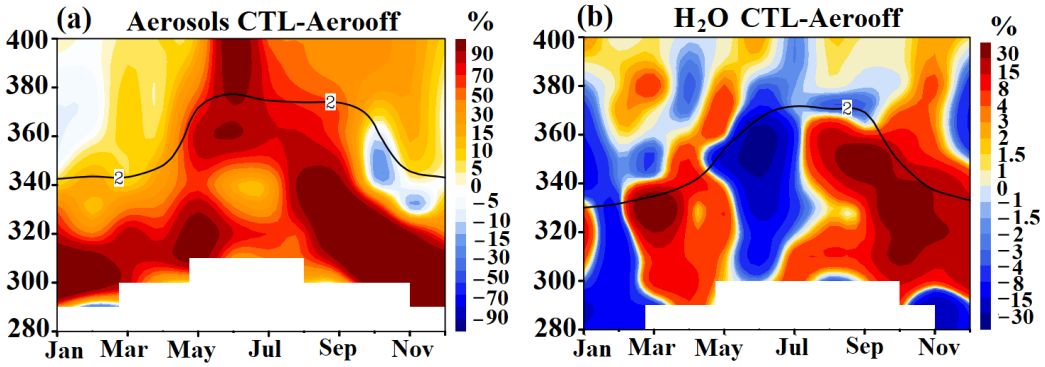

Figure 8: (a) Annual distribution of anomalies of aerosols (CTL - Aerooff) (averaged of BC, OC and sulfate aerosols) (%) averaged South Asian region (50° E – 100° E, 20° N – 40° N), (b) same as (a) but for water vapour (%) over North Indian-Ocean-Western-Pacific (30° E – 140° E, 20° N – 40° N. A black line in Figs. a-b indicates the dynamical tropopause.

Further, we analyze the correlation between heating rates and carbonaceous aerosol amounts in the UTLS (380 K level) in the Arctic during 2001 – 2016 (spring mean) (Fig. 9) from Aerooff, BCoff, and OCoff in comparison with CTL simulations. The carbonaceous aerosols show a positive correlation (correlation coefficient r: 0.55 to 0.85) with the UTLS heating rates indicating that transported carbonaceous aerosols enhance UTLS heating in the Arctic. It should be noted that increase in aerosols at the Arctic also occurs during the monsoon season (Fadnavis et al., 2017a, 2017b, 2019, Zheng et al., 2021) which may affect the dynamics and aerosol amounts in the spring of the next year in the UTLS.

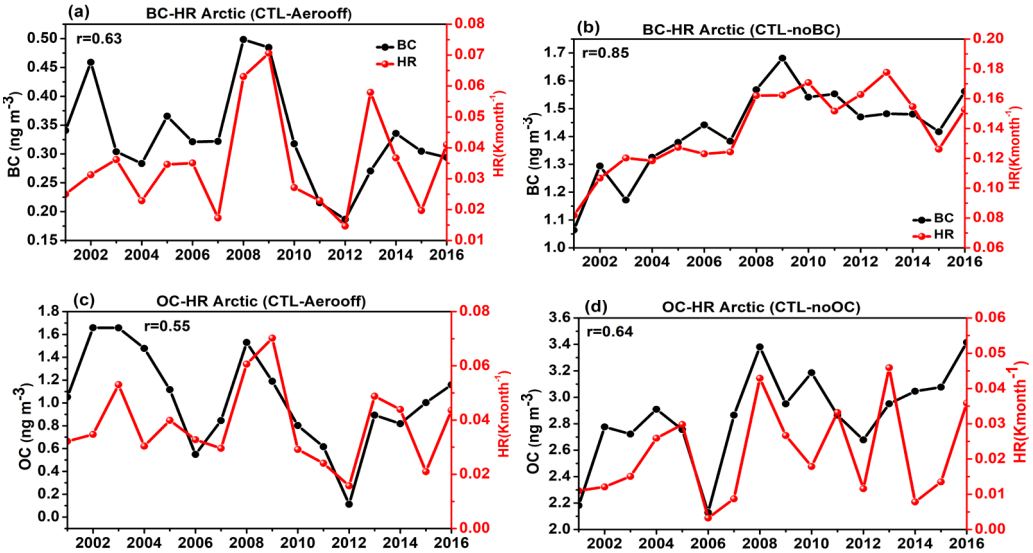

Figure 9: (a) Time series of BC aerosols and heating rates averaged for spring in the UTLS (380 K) in the Arctic (65° N – 85° N, 0 – 360°) (from CTL – Aerooff), (b) same as (a) but from CTL – BCoff. (c) same as (a) but for OC, (d) same as (c) but form CTL – OCoff. The correlation coefficient (r) between anomalies of BC/OC aerosols and heating rates is indicated in panels a-d.

Importantly, South Asian aerosols enhance water vapor in the lower stratosphere in the tropical and subtropical latitudes (45º S – 45º N). Water vapor being a greenhouse gas further enhances the heating of the troposphere leading to a positive feedback. The increase in water vapor in the stratosphere also warms the Earth's surface (Shindell, 2001; Solomon et al., 2010). Solomon et al. (2010) estimated that an increase in the stratospheric water vapor by 1 ppmv accounts for 0.24 W m^{-2} radiative forcing at the TOA. The SABER and MLS observations showed an increase in stratospheric water vapor by 0.45 ppmv globally during 2003 – 2017 (Yue et al., 2019). Thus the radiative forcing due to water vapor increase (0.02 – 0.14 ppmv) in response to South Asian anthropogenic aerosols is not negligible for surface warming globally. Further, increasing stratospheric water vapour could also lead to ozone depletion (e.g., Shindell, 2001, Robrecht et al., 2019).

4. Conclusions

A series of ECHAM6-HAMMOZ chemistry-climate simulations for South Asian anthropogenic aerosols were used to understand the transport pathways of South Asian aerosols in spring and their impacts on the UTLS. The model simulations show that large amounts of South Asian aerosols are transported during spring to the Arabian Sea (increases in AOD by: 0.02 – 0.12 from CTL - Aerooff) and Bay of Bengal (increases in AOD by: 0.16 to 0.8 from CTL - Aerooff) and Western Pacific (increases in AOD by 0.08 to 0.18). These aerosols are further lifted up into the UTLS from the North Indian Ocean and South Asia (10° N – 30° N). In the UTLS, they are also transported to the southern hemisphere (15° S – 30° S) and

471 downward (320K – 340K). The processes responsible for interhemispheric transport are as
472 follows:

473 (1) South Asian aerosols are lifted up to the UTLS by the ascending branch of Hadley
474 circulation. In the UTLS the aerosols enter the westerly Jet.

475 (2) They are transported to the Southern hemisphere via the Atlantic westerly duct (5° S – 5°
476 N, 10° W – 40° W) and Pacific westerly duct (5° S – 5° N, 50° E – 140° E),

477 (3) A shift in the Pacific westerly duct may be due to an increase in Rossby Wave Breaking
478 over the north Indian Ocean-western Pacific induced by South Asian aerosols.

479 The anthropogenic aerosol produces significant radiative impacts over the Indo-Gangetic Plain
480 (RF anomalies estimated from CTL-Aerooff simulations, TOA: +1.27±0.16 W m^{-2}, Surface: -
481 11.16±0.50 W m^{-2}, In-atmosphere: +12.44±0.42 W m^{-2}) and the Arabian Sea (RF at the TOA:
482 -0.72±0.14 W m^{-2}, surface: -3.00±0.28 W m^{-2}, In-atmosphere: +2.27±0.19 W m^{-2}).
483 Interestingly, RF at the TOA over the Indo-Gangetic Plain is positive (+4.33±0.17 W m^{-2}) due
484 to the emission of BC aerosols alone. The anthropogenic aerosols enhance heating in the
485 troposphere over the North Indian Ocean (estimated from CTL-Aerooff) by 0.15 to 0.4 K
486 $month^{-1}$ (4 – 60 %) and UTLS by 0.02 to 0.3 K $month^{-1}$ (10 – 60 %).

487 The heating of the troposphere by the carbonaceous aerosol (mainly BC) increases
488 temperature and thereby tropospheric water vapor amounts over the North Indian Ocean and
489 adjoining regions. The elevated water vapor is transported to the UTLS from the North Indian
490 ocean-western Pacific region (30° E – 140° E, 20° N – 40° N). In the UTLS it is transported
491 to the Southern Hemisphere ~45° S. BC aerosols play a major role in water vapor enhancement
492 in the lower stratosphere (increased water vapor by 0.8 – 5 %). As water vapour is a greenhouse
493 gas, this enhancement of stratospheric water vapour could potentially amplify the warming of

494 the troposphere and surface and cause a positive feedback (e.g. Shindell, 2001; Solomon et al.,
495 2010).

496 *Acknowledgments*: The authors thank the staff of the High Power Computing Centre (HPC) in
497 the Indian Institute of Tropical Meteorology, Pune, India, Pune, India. We thank the reviewers
498 for their valuable suggestions. We thank Jonathon Wright for useful discussions and
499 suggestions that improved the quality of the manuscript.

500 **Data availability:** The data used in this study are generated from ECHAM6-HAMMOZ model
501 simulations at the High-performance computing system in the Indian Institute of Tropical
502 Meteorology, Pune, India. The AOD data from MODIS Terra used here can be downloaded
503 from https://ladsweb.modaps.eosdis.nasa.gov/archive/allData/61/MODATML2/, and MISR
504 from https://misr.jpl.nasa.gov/getData/accessData/.
505
506 **Author contributions**: S. F. initiated the idea. A. J., S. S., A. A., performed model analysis.
507 R. M., and A. R. contributed to analysis and study design. All authors contributed to the writing
508 and discussions of the manuscript.
509
510 **Competing Interests**: Some authors are members of the editorial board of Atmospheric
511 Chemistry and Physics. The peer-review process was guided by an independent editor, and the
512 authors have also no other competing interests to declare.
513

514 **References:**

515 Aswini, A. R., Hegde, P., Aryasree, S., Girach, I. A. and Nair, P. R.: Continental outflow of
516 anthropogenic aerosols over Arabian Sea and Indian Ocean during wintertime: ICARB-
517 2018 campaign, Sci. Total Environ., 712, 135214, doi:10.1016/j.scitotenv.2019.135214,
518 2020.

519 Babu, S. S., Manoj, M. R., Moorthy, K. K., Gogoi, M. M., Nair, V. S., Kompalli, S. K.,
520 Satheesh, S. K., Niranjan, K., Ramagopal, K., Bhuyan, P. K. and Singh, D.: Trends in
521 aerosol optical depth over Indian region: Potential causes and impact indicators, J.
522 Geophys. Res. Atmos., 118, 11,794-11,806, doi:10.1002/2013JD020507, 2013.

523 Budhavant, K., Bikkina, S., Andersson, A., Asmi, E., Backman, J., Kesti, J., Zahid, H.,
524 Satheesh, S. K. and Gustafsson, Ö.: Anthropogenic fine aerosols dominate the wintertime
525 regime over the northern Indian Ocean, Tellus, Ser. B Chem. Phys. Meteorol., 70, 1–15,
526 doi:10.1080/16000889.2018.1464871, 2018.

527 Chavan, P., Fadnavis, S., Chakroborty, T., Sioris, C. E. and Müller, R.: The outflow of Asian
528 biomass burning carbonaceous aerosol into the UTLS in spring: Radiative effects seen in
529 a global model, 21, 14371–14384, https://doi.org/10.5194/acp-2021-494, 2021.

530 Corrigan, C. E., Roberts, G. C., Ramana, M. V., Kim, D. and Ramanathan, V.: Capturing
531 vertical profiles of aerosols and black carbon over the Indian Ocean using autonomous
532 unmanned aerial vehicles, Atmos. Chem. Phys., 8, 737–747, doi:10.5194/acp-8-737-
533 2008, 2008.

534 Collins, M., Sutherland, M., Bouwer, L., Cheong, S.-M., Frölicher, T. L., Jacot Des Combes,
535 H., Roxy, M. K., Losada, I., McInnes, K. L., Ratter, B., Rivera-Arriaga, E., Susanto, R.
536 D., Swingedouw, D., Tibig, L., Bakker, P., Eakin, C. M., Emanuel, K., Grose, M., Hemer,
537 M., Jackson, L., Kääb, A., Kajtar, J. B., Knutson, T., Laufkötter, C., Noy, I., Payne, M.,

Ranasinghe, R., Sgubin, G. and Timmermans, M.-L.: Extremes, Abrupt Changes and Managing Risks, IPCC Spec. Rep. Ocean Cryosph. a Chang. Clim., 589–655, 2019.

De Reus, M., Krejci, R., Williams, J., Fischer, H., Scheele, R. and Ström, J.: Vertical and horizontal distributions of the aerosol number concentration and size distribution over the northern Indian Ocean, J. Geophys. Res. Atmos., 106, 28629–28641, doi:10.1029/2001JD900017, 2001.

Dickerson, R. R., Andreae, M. O., Campos, T., Mayol-Bracero, O. L., Neususess, C. and Streets, D. G.: Analysis of black carbon and carbon monoxide observed over the Indian Ocean: Implications for emissions and photochemistry, J. Geophys. Res. Atmos., 107, doi:10.1029/2001JD000501, 2002.

Fadnavis, S., Kalita, G., Rowlinson, M., Rap, A., Li, J.-L. F., Gasparini, B., Laakso, A. and Müller, R.: The impact of increases in South Asian anthropogenic emissions of SO_2 on sulfate loading in the upper troposphere and lower stratosphere during the monsoon season and the associated radiative changes, Atmos. Chem. Phys., 19, 9989–10008, https://doi.org/10.5194/acp-19-9989-2019, 2019.

Fadnavis, S., Roy, C., Sabin, T. P., Ayantika, D. C. and Ashok, K.: Potential modulations of pre-monsoon aerosols during El Niño: impact on Indian summer monsoon, Clim. Dyn., 49, 2279–2290, doi:10.1007/s00382-016-3451-6, 2017a.

Fadnavis, S., Kalita, G., Ravi Kumar, K., Gasparini, B. and Li, J. L. F.: Potential impact of carbonaceous aerosol on the upper troposphere and lower stratosphere (UTLS) and precipitation during Asian summer monsoon in a global model simulation, Atmos. Chem. Phys., 17, 11637–11654, doi:10.5194/acp-17-11637-2017, 2017b.

Fadnavis, S. and Chattopadhyay, R.: Linkages of subtropical stratospheric intraseasonal intrusions with Indian summer monsoon deficit rainfall, J. Clim., 30, 5083–5095,

562 doi:10.1175/JCLI-D-16-0463.1, 2017.

563 Fadnavis, S., Semeniuk, K., Pozzoli, L., Schultz, M. G., Ghude, S. D., Das, S. and Kakatkar,
564 R.: Transport of aerosols into the UTLS and their impact on the asian monsoon region as
565 seen in a global model simulation, Atmos. Chem. Phys., 13, 8771–8786,
566 doi:10.5194/acp-13-8771-2013, 2013.

567 Fadnavis, S., Sabin, T. P., Rap, A., Müller, R., Kubin, A. and Heinold, B.: The impact of
568 COVID-19 lockdown measures on the Indian summer monsoon, Environ. Res. Lett.,
569 16, 074054, doi:10.1088/1748-9326/ac109c, 2021a.

570 Fadnavis S., Müller R , Chakraborty T. , Sabin T. P., Laakso A. , Rap A. , Griessbach S.,
571 Vernier J-P., and Tilmes S., The role of tropical volcanic eruptions in exacerbating
572 Indian droughts, Sci. Rep., 11, 2714, doi.org/10.1038/s41598-021-81566-0, 2021b.

573 Frederiksen, J. S. and Francey, R. J.: Unprecedented strength of Hadley circulation in 2015–
574 2016 impactson CO2 interhemispheric difference, Atmos. Chem. Phys., 18, 14837–
575 14850, https://doi.org/10.5194/acp-18-14837-2018, 2018.

576 Holton, J. R., Haynes, P. H., McIntyre, M. E., Douglass, A. R., Rood, R. B., Pfister, L.:
577 Stratosphere-troposphere exchange, Reviews of Geophysics, 33, 403-439,
578 https://doi.org/10.1029/95RG02097, 1995.

579 Jose, S., Nair, V. S. and Babu, S. S.: Anthropogenic emissions from South Asia reverses the
580 aerosol indirect effect over the northern Indian Ocean, Sci. Rep., 10, 18360,
581 doi:10.1038/s41598-020-74897-x, 2020.

582 Karambelas, A., Holloway, T., Kinney, P. L., Fiore, A. M., Defries, R., Kiesewetter, G. and
583 Heyes, C.: Urban versus rural health impacts attributable to PM2.5 and O_3 in northern
584 India, Environ. Res. Lett., 13, 064010, doi:10.1088/1748-9326/aac24d, 2018.

585 Kahn, R. A., Garay, M. J., Nelson, D. L., Yau, K. K., Bull, M. A., Gaitley, B. J., Martonchik,

586 J. V., and Levy, R. C.: Satellite-derived aerosol optical depth over dark water from MISR
587 and MODIS: Comparisons with AERONET and implications for climatological studies,
588 J. Geophys. Res.,112, D18205, doi:10.1029/2006JD008175, 2007.

589 Kunz, A., Konopka, P., Müller, R. and Pan, L. L.: The dynamical tropopause based on
590 isentropic potential vorticity gradients J. Geophys. Res., 116, D01110,
591 doi:10.1029/2010JD014343,2011.

592 Lu, Z., Zhang, Q. and Streets, D. G.: Sulfur dioxide and primary carbonaceous aerosol
593 emissions in China and India, 1996-2010, Atmos. Chem. Phys., 11, 9839–9864,
594 doi:10.5194/acp-11-9839-2011, 2011.

595 Mahowald, N. M., Hamilton, D. S., Mackey, K. R. M., Moore, J. K., Baker, A. R., Scanza, R.
596 A. and Zhang, Y.: Aerosol trace metal leaching and impacts on marine microorganisms,
597 Nat. Commun., 9, 2614, doi:10.1038/s41467-018-04970-7, 2018.

598 Mayol-Bracero, O. L., Gabriel, R., Andreae, M. O., Kirchstetter, T. W., Novakov, T., Ogren,
599 J., Sheridan, P. and Streets, D. G.: Carbonaceous aerosols over the Indian Ocean during
600 the Indian Ocean Experiment (INDOEX): Chemical characterization, optical properties,
601 and probable sources, J. Geophys. Res. Atmos., 107, 8030, doi:10.1029/2000JD000039,
602 2002.

603 McFarquhar, G. M. and Wang, H.: Effects of aerosols on trade wind cumuli over the Indian
604 Ocean: Model simulations, Q. J. R. Meteorol. Soc., 132, 821–843, doi:10.1256/qj.04.179,
605 2006.

606 Meehl, G. A., Arblaster, J. M. and Collins, W. D.: Effects of black carbon aerosols on the
607 Indian monsoon, J. Clim., 21, 2869–2882, doi:10.1175/2007JCLI1777.1, 2008.

608 Nair, V. S., Babu, S. S., Manoj, M. R., Moorthy, K. K. and Chin, M.: Direct radiative effects

of aerosols over South Asia from observations and modeling, Clim. Dyn., 49, 1411–1428, doi:10.1007/s00382-016-3384-0, 2017.

Neubauer, D., Lohmann, U., Hoose, C. and Frontoso, M. G.: Impact of the representation of marine stratocumulus clouds on the anthropogenic aerosol effect, Atmos. Chem. Phys., 14, 11997–12022, doi:10.5194/acp-14-11997-2014, 2014.

Paliwal, U., Sharma, M. and Burkhart, J. F.: Monthly and spatially resolved black carbon emission inventory of India: Uncertainty analysis, Atmos. Chem. Phys., 16, 12457–12476, doi:10.5194/acp-16-12457-2016, 2016.

Papaspiropoulos, G., Martinsson, B. G., Zahn, A., Brenninkmeijer, C. A. M., Hermann, M., Heintzenberg, J., Fischer, H. and Van Velthoven, P. F. J.: Aerosol elemental concentrations in the tropopause region from intercontinental flights with the Civil Aircraft for Regular Investigation of the Atmosphere Based on an Instrument Container (CARIBIC) platform, J. Geophys. Res. Atmos., 107, 4671, doi:10.1029/2002JD002344, 2002.

Pathak, H. S., Satheesh, S. K., Moorthy, K. K. and Nanjundiah, R. S.: Assessment of regional aerosol radiative effects under the SWAAMI campaign - Part 2: Clear-sky direct shortwave radiative forcing using multi-year assimilated data over the Indian subcontinent, Atmos. Chem. Phys., 20, 14237–14252, doi:10.5194/acp-20-14237-2020, 2020.

Penner, J. E., Chuang, C. C. and Grant, K.: Climate forcing by carbonaceous and sulfate aerosols, Clim. Dyn., 14, 839–851, doi:10.1007/s003820050259, 1998.

Ploeger, F., Konopka, P., Walker, K., and Riese, M.: Quantifying pollution transport from the Asian monsoon anticyclone into the lower stratosphere, Atmos. Chem. Phys., 17, 7055–7066, https://doi.org/10.5194/acp-17-7055-2017, 2017.

633 Rajeev, K. and Ramanathan, V.: Direct observations of clear-sky aerosol radiative forcing from
634 space during the Indian Ocean Experiment, J. Geophys. Res. Atmos., 106, 17221–17235,
635 doi:10.1029/2000JD900723, 2001.

636 Ramachandran, S., Rupakheti, M. and Lawrence, M. G.: Aerosol-induced atmospheric heating
637 rate decreases over South and East Asia as a result of changing content and composition,
638 Sci. Rep., 10, 20091, doi:10.1038/s41598-020-76936-z, 2020a.

639 Ramachandran, S., Rupakheti, M. and Lawrence, M. G.: Black carbon dominates the aerosol
640 absorption over the Indo-Gangetic Plain and the Himalayan foothills, Environ. Int., 142,
641 105814, doi:10.1016/j.envint.2020.105814, 2020b.

642 Ramanathan, V., Chung, C., Kim, D., Bettge, T., Buja, L., Kiehl, J. T., Washington, W. M.,
643 Fu, Q., Sikka, D. R. and Wild, M.: Atmospheric brown clouds: Impacts on South Asian
644 climate and hydrological cycle, Proc. Natl. Acad. Sci. U. S. A., 102, 5326–5333,
645 doi:10.1073/pnas.0500656102, 2005.

646 Ramanathan, V., Crutzen, P. J., Lelieveld, J., Mitra, A. P., Althausen, D., Anderson, J.,
647 Andreae, M. O., Cantrell, W., Cass, G. R., Chung, C. E., Clarke, A. D., Coakley, J. A.,
648 Collins, W. D., Conant, W. C., Dulac, F., Heintzenberg, J., Heymsfield, A. J., Holben,
649 B., Howell, S., Hudson, J., Jayaraman, A., Kiehl, J. T., Krishnamurti, T. N., Lubin, D.,
650 McFarquhar, G., Novakov, T., Ogren, J. A., Podgorny, I. A., Prather, K., Priestley, K.,
651 Prospero, J. M., Quinn, P. K., Rajeev, K., Rasch, P., Rupert, S., Sadourny, R., Satheesh,
652 S. K., Shaw, G. E., Sheridan, P. and Valero, F. P. J.: Indian Ocean Experiment: An
653 integrated analysis of the climate forcing and effects of the great Indo-Asian haze, J.
654 Geophys. Res. Atmos., 106, 28371–28398, doi:10.1029/2001JD900133, 2001.

655 Robrecht, S., Vogel, B., Grooß, J.-U., Rosenlof, K., Thornberry, T., Rollins, A., Krämer, M.,
656 Christensen, L. and Müller, R.: Mechanism of ozone loss under enhanced water vapour

conditions in the mid-latitude lower stratosphere in summer, Atmos. Chem. Phys., 19, 5805–5833, doi:10.5194/acp-19-5805-2019, 2019.

Romatschke, U. and Houze, R. A.: Characteristics of precipitating convective systems in the South Asian monsoon, J. Hydrometeorol., 12, 3–26, doi:10.1175/2010JHM1289.1, 2011.

Satheesh, S. K., Ramanathan, V., Holben, B. N., Krishna Moorthy, K., Loeb, N. G., Mating, H., Prospero, J. M. and Savoie, D.: Chemical, microphysical, and radiative effects of Indian Ocean aerosols, J. Geophys. Res., 107, 4725, doi:10.1029/2002JD002463, 2002.

Satheesh, S. K. and Ramanathan, V.: Large differences in tropical aerosol forcing at the top of the atmosphere and Earth's surface, Nature, 405, 60–63, doi:10.1038/35011039, 2000.

Shindell, D. T.: Climate and ozone response to increased stratospheric water vapor, Geophys. Res. Lett., 28, 1551–1554, doi:10.1029/ 1999GL011197, 2001.

Solomon, S., Rosenlof, K. H., Portmann, R. W., Daniel, J. S., Davis, S. M., Sanford, T. J. and Plattner G. K.: Contributions of stratospheric water vapor to decadal changes in the rate of global warming, Science, 327, 1219–1223, 0.1126/science.1182488, 2010.

Shindell, D. T., Chin, M., Dentener, F., Doherty, R. M., Faluvegi, G., Fiore, A. M., Hess, P., Koch, D. M., MacKenzie, I. A., Sanderson, M. G., Schultz, M. G., Schulz, M., Stevenson, D. S., Teich, H., Textor, C., Wild, O., Bergmann, D. J., Bey, I., Bian, H., Cuvelier, C., Duncan, B. N., Folberth, G., Horowitz, L. W., Jonson, J., Kaminski, J. W., Marmer, E., Park, R., Pringle, K. J., Schroeder, S., Szopa, S., Takemura, T., Zeng, G., Keating, T. J., and Zuber, A.: A multi-model assessment of pollution transport to the Arctic, Atmos. Chem. Phys., 8, 5353–5372, https://doi.org/10.5194/acp-8-5353-2008, 2008.

Stier, P., Feichter, J., Kinne, S., Kloster, S., Vignati, E., Wilson, J., Ganzeveld, L., Tegen, I., Werner, M., Balkanski, Y., Schulz, M., Boucher, O., Minikin, A., and Petzold, A.: The

680 aerosol-climate model ECHAM5-HAM, Atmos. Chem. Phys., 5, 1125–1156,
681 doi:10.5194/acp-5-1125-2005, 2005.

682 Taylor, K. E., Williamson, D. L. and Zwiers, F. W.: The Sea Surface Temperature and Sea-Ice
683 Concentration Boundary Conditions for AMIP II Simulations, Program for Climate
684 Model Diagnosis and Intercomparison (PCMDI), Lawrence Livermore Natl. Lab.
685 Livermore, Calif., Rep., 60, 1–28 http://www-pcmdi.llnl.gov/publications/ab60.html,
686 2000.

687 Tegen, I., Neubauer, D., Ferrachat, S., Drian, C. S. Le, Bey, I., Schutgens, N., Stier, P., Watson-
688 Parris, D., Stanelle, T., Schmidt, H., Rast, S., Kokkola, H., Schultz, M., Schroeder, S.,
689 Daskalakis, N., Barthel, S., Heinold, B. and Lohmann, U.: The global aerosol-climate
690 model echam6.3-ham2.3 -Part 1: Aerosol evaluation, Geosci. Model Dev., 12, 1643–
691 1677, doi:10.5194/gmd-12-1643-2019, 2019.

692 Tegen, I., Harrison, S. P., Kohfeld, K. E., Prentice, I. C., Coe, M., and Heimann, M.: Impact of
693 vegetation and preferential source areas on global dust aerosol: Results from a model
694 study, J. Geophys. Res.-Atmos., 107, 14–27, https://doi.org/10.1029/2001JD000963,
695 2002.

696 Waugh, D. W. and Polvani, L. M.: Intrusions into the tropical upper troposphere, Geophys.
697 Res. Lett., 27, 3857–3860, https://doi.org/10.1029/2000GL012250, 2000.

698 Yan, X., Konopka, P., Hauck, M., Podglajen, A., and Ploeger, F.: Asymmetry and pathways of
699 inter-hemispheric transport in the upper troposphere and lower stratosphere, Atmos.
700 Chem. Phys., 21, 6627–6645, https://doi.org/10.5194/acp-21-6627-2021, 2021.

701 Yue, J., Russell, J., Gan, Q., Wang, T., Rong, P., Garcia, R. and Mlynczak, M.: Increasing
702 Water Vapor in the Stratosphere and Mesosphere After 2002, Geophys. Res. Lett., 46,

13452–13460, doi:10.1029/2019GL084973, 2019.

Zhang, K., O'Donnell, D., Kazil, J., Stier, P., Kinne, S., Lohmann, U., Ferrachat, S., Croft, B., Quaas, J., Wan, H., Rast, S. and Feichter, J.: The global aerosol-climate model ECHAM-HAM, version 2: Sensitivity to improvements in process representations, Atmos. Chem. Phys., 12, 8911–8949, doi:10.5194/acp-12-8911-2012, 2012.

Zheng, C., Wu, Y., Ting, M., Orbe, C., Wang, X., and Tilmes, S.: Summertime transport pathways from different northern hemisphere regions into the Arctic. Journal of Geophysical Research: Atmospheres, 126, e2020JD033811. https://doi. org/10.1029/2020JD033811, 2021